Applied Catalysis B: Environmental 219 (2017) 92–100

Contents lists available at ScienceDirect

Applied Catalysis B: Environmental

journal homepage: www.elsevier.com/locate/apcatb

# Boron doped graphitic carbon nitride with acid-base duality for cycloaddition of carbon dioxide to epoxide under solvent-free condition

Junjiang Zhu[a,b,**], Tingting Diao[a], Wenyao Wang[b], Xuelian Xu[a], Xiaoying Sun[a], Sónia A.C. Carabineiro[c,*], Zhen Zhao[a,*]

[a] Institute of Catalysis for Energy and Environment, College of Chemistry and Chemical Engineering, Shenyang Normal University, 523 Huanghe North Street, Shenyang 110034, China

[b] Key Laboratory of Catalysis and Materials Science of the State Ethnic Affairs Commission & Ministry of Education, South-Central University for Nationalities, 182 Minzudadao, Wuhan 430074, China

[c] Laboratory of Catalysis and Materials (LCM), Associate Laboratory LSRE/LCM, Department of Chemical Engineering, Faculty of Engineering, University of Porto, Rua Dr. Roberto Frias, 4200-465 Porto, Portugal

ARTICLE INFO

*Article history:*
Received 23 April 2017
Received in revised form 9 July 2017
Accepted 15 July 2017
Available online 18 July 2017

*Keywords:*
Carbon nitride
Boron doping
Acid-base duality
$CO_2$ cycloaddition
Reaction mechanism
DFT calculations

ABSTRACT

The cycloaddition of $CO_2$ and epoxides to yield cyclic carbonate under solvent-free conditions is an eco-friendly way to utilize $CO_2$ in environmental science and green chemistry. In this paper, we report that boron doped carbon nitride (BCN) is highly active and selective for such reactions. BCN, especially if supported on mesoporous silica SBA-15 (i.e., $B_{0.1}$CN/SBA-15), shows above 95% conversion and selectivity for cycloaddition of $CO_2$ and styrene oxide (SO) to yield styrene carbonate (SC), even under solvent-free conditions. That is mainly due to the acid-base duality induced by B doping, which enables the co-activation of $CO_2$ and epoxide. A mechanism based on acid-base duality is proposed, where $CO_2$ is activated on the basic >NH sites and SO is on the acidic $-B(OH)_2$ sites through a hydrogen bonding. The co-activated $CO_2$ and SO react with each other to yield the SC. Density functional theory (DFT) calculations were conducted to support the mechanism, which show that the co-adsorption of $CO_2$ and SO on BCN is energetically favorable and the reaction follows the Langmuir-Hinshelwood mechanism. The BCN with acid-base duality provides an option for cheap, green and efficient catalysts for $CO_2$ utilization.



## 1. Introduction

Carbon dioxide ($CO_2$) is not only a greenhouse gas that greatly contributes to the global warming, but also a cheap, nontoxic and abundant C1 building block for the synthesis of fine chemicals [1]. The conversion of $CO_2$ into chemical feedstocks can enter the natural carbon cycle and reduce global energy and environmental problems [2]. Cycloaddition of $CO_2$ and epoxides to produce cyclic carbonate (see Scheme 1 for example) is one of the attracting routes for $CO_2$ utilization, which not only eliminates $CO_2$, but also provides a green path for the synthesis of chemical intermediates in fine chemistry. This technology however remains still a challenge in terms of practical applications, because $CO_2$ is thermodynamically and kinetically stable and its activation needs a large energy input [3]. The search for green catalysts that can actively and selectively convert $CO_2$ to the desired products is a crucial key for $CO_2$ utilization.

Molecular orbital theory points out that $CO_2$ has a low-level empty orbital ($2\pi^*$) with a bond order of 2, which can be decreased if $CO_2$ attracts external electrons to the $2\pi^*$ orbital, facilitating $CO_2$ activation. This shows that materials having electron-rich structure and capability of donating electrons can be potential catalysts for $CO_2$ activation, as is also known in literature [4–7]. In this work, relying on our previous achievements [8–12], we chose polymeric carbon nitride (CN) for investigation. CN has been found to be a promising catalyst for various reactions, including photocatalysis [13–21], fine chemicals synthesis [22–25], $CO_2$ activation [26–30], etc., due to the dramatic electronic band structures and surface-rich Lewis basicity. In particular, CN is a metal-free solid

* Corresponding authors.
** Corresponding author at: Key Laboratory of Catalysis and Materials Science of the State Ethnic Affairs Commission & Ministry of Education, South-Central University for Nationalities, 182 Minzudadao, Wuhan 430074, China.
*E-mail addresses:* ciaczjj@163.com (J. Zhu), scarabin@fe.up.pt (S.A.C. Carabineiro), zhenzhao@cup.edu.cn (Z. Zhao).

http://dx.doi.org/10.1016/j.apcatb.2017.07.041
0926-3373/

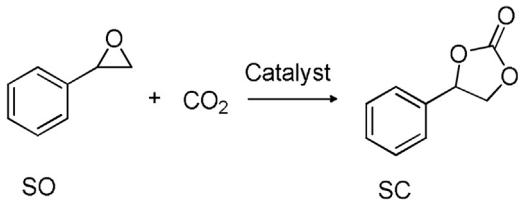


**Scheme 1.** Cycloaddition of $CO_2$ and styrene oxide to produce styrene carbonate.

material, thus no attention needs to pay on the metal contamination compared to metal-containing catalysts, and on the separation of catalyst/product compared to organic or ionic liquid catalysts.

On the other hand, it was recently reported that boronic acid is an efficient organocatalyst for the activation of epoxides because of its Lewis acid properties [31]. This made us wonder if it would be possible to combine boric acid with CN, by an in-situ method, to form a Lewis base-Lewis acid coalition, and use it as catalyst for the co-activation of $CO_2$ and epoxide, to promote the reaction. Co-activation of the reactants is more likely in catalysis according to the Langmuir-Hinshelwood mechanism [32–34].

In this work, we synthesize boron doped carbon nitrides with varied B dopings ($B_r$CN) and use them as catalysts for cycloaddition of $CO_2$ and styrene oxide (SO) to yield styrene carbonate (SC) conducted under solvent-free conditions. The results indicate for the first time that doping of B atoms can significantly increase both the surface basic and acid sites of g-CN, which are adsorption and active sites for $CO_2$ and epoxide, respectively [6,35]. Therefore, a significant improvement in the $CO_2$ cycloaddition activity is observed, comparing CN to $B_r$CN. The activity can be further improved if the material is supported on high-surface-area ordered mesoporous silica SBA-15 (i.e., $B_r$CN/SBA-15), with both SO conversion and SC selectivity above 95%. A mechanism based on acid-base duality is proposed, where $CO_2$ is activated on the basic >NH sites and SO is on the acidic $-B(OH)_2$ sites through a hydrogen bonding. This is energetically supported by the density functional theory (DFT) calculations.

## 2. Experimental

### 2.1. Synthesis procedures for the materials

Mesoporous silica SBA-15, Fe-CN and Zn-CN were synthesized according to the procedures reported by Zhao et al. [36] and Wang et al. [37], and for simplicity, were not described here.

$B_r$CN with varied B dopings was synthesized according to literature [38]: Briefly, 2 g dicyandiamide and desired amount of $B(OH)_3$ (*e.g.*, 0.2 g for $B_{0.1}$CN) were added to 15 mL deionized water, heated and stirred at 80 °C, until all the water was evaporated. A white solid was obtained after the water evaporation, which was then transferred to a nitrogen oven and heated at 600 °C for 4 h (heating rate of 2 °C $min^{-1}$). Depending on the amount of $B(OH)_3$ added, the sample was denoted as $B_r$CN, where *r* represents the mass ratio of boric acid to dicyandiamide.

$B_r$CN/SBA-15 composites were prepared as below: 2 g dicyandiamide and desired amount of $B(OH)_3$ were dissolved in 15 mL deionized water and heated at 80 °C with stirring, to which 1 g SBA-15 was added. The mixture was continually stirred at 80 °C and white solid was obtained after water evaporation. The solid was calcined in a nitrogen oven at 600 °C for 4 h (heating rate of 2 °C $min^{-1}$), yielding the product $B_r$CN/SBA-15, where *r* has the same mean as that in *$B_r$CN*.

The weight percentage of B atoms in $B_{0.03}$CN and $B_{0.1}$CN/SBA-15 (the best two samples tested in the catalytic reactions), determined by TG measurements (see Fig. S**1**), is 1.09% and 1.61%. For convenience, we used the nominal weight ratio of B atoms, for easier description in the context. For example, $B_{0.03}$CN means that the sample was prepared using 2 g dicyandiamide and 0.06 g $B(OH)_3$.

### 2.2. Characterizations

X-ray diffraction (XRD) patterns were obtained on a Bruker D8 Advance X-ray diffractometer with Cu Kα (λ = 1.5406 Å) irradiation. Fourier transformed infrared (FTIR) spectra were recorded on a Nicolet 470 FTIR spectrometer, working in the range of 400–4000 $cm^{-1}$ at a resolution of 0.09 $cm^{-1}$. Transmission electron microscopy (TEM) images were obtained on a Tecnai $G^2$ 20 S-Twin apparatus with high-resolution transmission electron microscope (200 kV). Before observation the sample was first dispersed in ethanol by ultrasonic method, and then deposited on a copper mesh. $N_2$ adsorption/desorption isotherms were measured on a TriStar II 3020 measurement at liquid nitrogen temperature. Before measurement the sample was treated in vacuum at 150 °C for 5 h. X-ray photoelectron spectroscopy (XPS) spectra were recorded on a VG Multi lab 2000 apparatus using a monochromatic Al K*a* X-ray source (300 W) and analyser pass energy of 25 eV. Binding energies were obtained by referencing to the C1 s binding energy (284.6 eV).

Temperature-programmed desorption (TPD) of $CO_2$ and $NH_3$ were measured on a homemade TPD apparatus equipped with a thermal conductivity detector (TCD), as follows. The sample (0.1 g) was first treated in Helium at 300 °C for 1 h and then cooled to room temperature. $CO_2/NH_3$ was subsequently switched to the sample for adsorption for 30 min. Thereafter, Helium with flow rate of 30 mL $min^{-1}$ was switched again to the sample, and after reaching a stable baseline, the sample was heated from RT to 500 °C at a heating rate of 10 °C $min^{-1}$ to record the profile.

### 2.3. Catalytic tests

1 mL styrene oxide and 30 mg catalysts were mixed in a 25 mL stainless steel high pressure reactor. The reactor was sealed and flushed 5 times with $CO_2$ at room temperature to remove air from the vessel. The pressure was then adjusted to 3 MPa and the reactor heated to 130 °C. The reaction was initialized by stirring (500 rpm) under the pressurized conditions. After reaction, the reactor was quickly cooled in cold water, and pressure was slowly lowered. The reaction mixture was dissolved in dichloromethane ($CH_2Cl_2$) and the catalyst was separated by filtration. The filtrate containing reactant, product and internal standard (biphenyl, which was added after the separation of catalyst) was analysed on an Agilent GC equipped with HP-5 column and flame ionization detector (FID), to determine the reaction conversion and selectivity.

## 3. Results and discussion

### 3.1. Characterizations of the catalysts

XRD results show the characteristic diffraction peak of CN at 2θ = 27.4° for all samples, independently of the B doping, see Fig. 1**A**, indicating that the layered structure, analogous to the pure polymeric carbon nitride[39], is formed. However, the peak intensity decreases with the B doping, and the peak almost disappears at *r* = 0.2, suggesting that the $B(OH)_3$ addition restrains the polymerization of dicyandiamide, and less condensed $B_r$CN is formed. Considering that the condensation is based mainly on the edged amino and/or amine functionalities, a possible termination mechanism caused by $B(OH)_3$ addition is proposed, Fig. S**2**, showing the formation of $>NB(OH)_2$ group, which cause the termination step. Gouin et al. [40] reported that $B(OH)_3$ can react with $NH_3$ and form $H_2NB(OH)_2$ at temperatures below 600 °C, which supports that the $>NB(OH)_2$ group is formed on CN by reacting with the >NH functions. It is possible that the B atoms enter into the

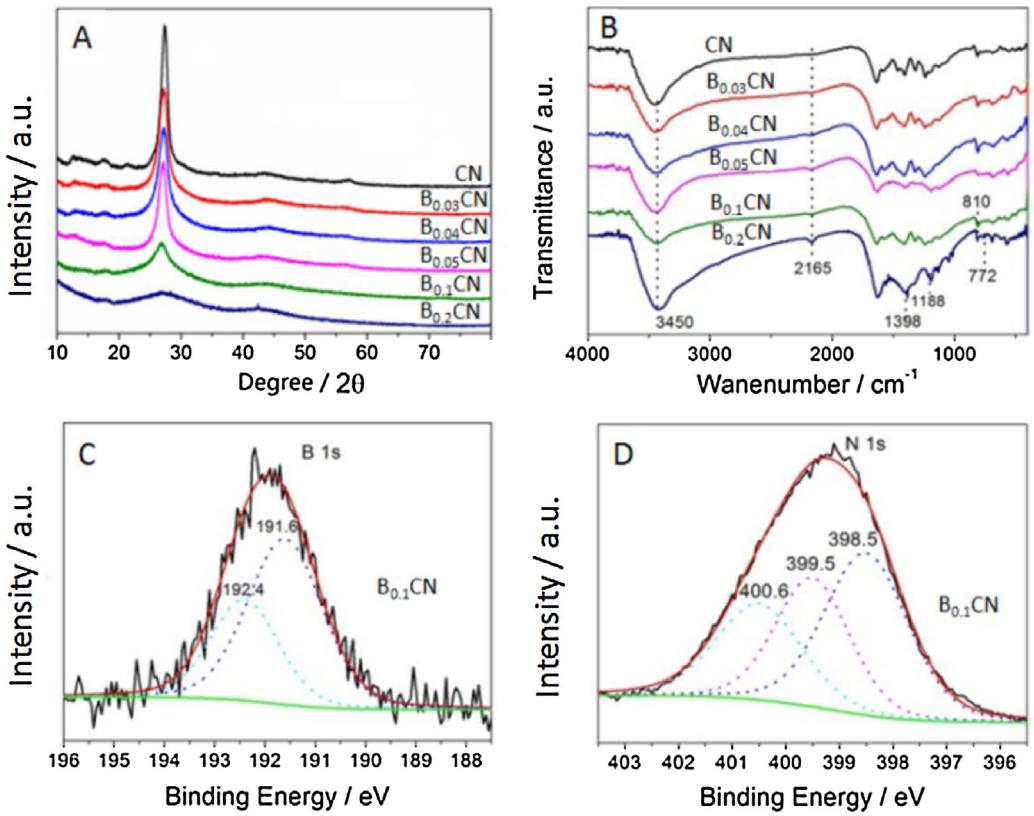


**Fig. 1.** XRD patterns (A) and FT-IR spectra (B) of the $B_rCN$ ($0 \le r \le 0.2$), where $r$ is the weight ratio of B to CN precursors; and the XPS spectra for B 1s (C) and N 1s (D) of $B_{0.1}CN$.

C—N—C six-membered rings, but this has no relation to the termination step. Although the treatment temperature (550 °C) is high enough to decompose $B(OH)_3$ into $B_2O_3$, no peak assignable to $B_2O_3$ is observed even at $r = 0.2$, suggesting that the B atoms exist mainly on the surface $>NB(OH)_2$ groups or in the C—N—C rings. Even for $B_2O_3$, Yan et al. and Li et al. reported that it can react with the C—$NH_2$ and 2C—NH groups of CN at temperatures above 520 °C, and can increase the thermal stability of CN [38,41], supporting our results. The formation of $>NB(OH)_2$ groups and BCN rings is also confirmed by FT-IR and XPS results, as will be shown later. For $B_rCN$/SBA-15, the peak intensity is significantly attenuated and decreases with B doping (Fig. S**3A**), due to the lower overall $B_rCN$ mass in the composite, as seen in a previous work dealing with g-CN/SBA-15 [8].

FT-IR spectra (Fig. 1**B**) confirm the formation of CN and B-containing functionalities. From previous literature [9,42–44], we know that the absorption bands at 810 $cm^{-1}$ and 1100–1650 $cm^{-1}$ are assigned to the stretch and bend vibration of C—N and/or C═N bonds of the tri-s-triazine rings, the band at 2165 $cm^{-1}$ being assigned to the stretch vibration of C≡N band and that at 1398 $cm^{-1}$ to the stretch vibrations of the B-N (B-O) bond [45]. The vibrations of the N—H bond at near 1600 $cm^{-1}$ and 3450 $cm^{-1}$, and that of B—O—H bond [46,47] at near 1150 $cm^{-1}$ are not clearly observed; they are presumably overlapped by the vibrations of the —OH ($H_2O$) and C—N bonds. For $B_rCN$/SBA-15, the bands attributed to BCN, SBA-15 (Si-O-Si) and —OH vibrations are present (Fig. S**3B**), suggesting that BCN is formed and the structure of SBA-15 is not destroyed.

To confirm the presence of B atoms and check its chemical status in the BCN material, XPS measurements were performed. The overall spectra show clearly the presence of B and O atoms, besides C and N atoms, Fig. S**4**. For B 1s, two peaks centred at 191.6 and 192.4 eV are fitted, Figs. 1**C**. The peak at 191.6 eV can be ascribed to the B atoms in BCN network, as indicated by Wang et al. [48] This binding energy is in between that for *h*-BN (190.6 eV) [49] and Kawaguchi's BCN(H) [50], where boron is surrounded by three N atoms (192.1 eV). Thus, existed in the BCN network are mainly Bay B atoms, which connects to the bridged N atoms (i.e., N-$(C)_3$, where one carbon was replaced by boron) [48]. The peak at 192.4 eV can be ascribed to the boron atoms surrounded by one N atom and two O atoms (e.g., N-$B(OH)_2$), according to Cholet et al. [49]. This supports the formation of $>NB(OH)_2$ group shown in the termination mechanism, Fig. S**2**.

For N 1s spectra, three peaks can be fitted, with the peak at 398.5 eV being ascribed to the N atoms in the BCN network [40], that at 399.5 eV to the N atoms in —$NH_2$, >NH or >NB groups [51], and that at 400.6 eV to the N atoms in N-$(C)_3$ groups [38], Fig. 1**D**. Moreover, the binding energies of C 1s (288.4 eV) and O 1s (531.9 eV) also support that the CN networks and the B-O bonds are formed, see Fig. S**4**. That is, the BCN networks, as well as the surface —$NH_2$, >NH and $>NB(OH)_2$ groups, are formed. It is worth noting that the binding energies of C 1s, N 1s and B1s shift slightly to higher values comparing BCN to BCN/SBA-15. Since SBA-15 is an inert support and should not interact strongly with BCN, we believe that this is caused by the increase of surface area, which changes the surface energy and hence the binding energy of the material.

Further characterizations from $N_2$ physisorption and TGA and B-NMR measurements show that the surface area largely increases from 14 $m^2/g$ for $B_{0.1}CN$ to 123 $m^2/g$ for $B_{0.1}CN$/SBA-15, the loading of $B_{0.1}CN$ in $B_{0.1}CN$/SBA-15 is 40 wt.% in weight (see Fig. S**5**), and the B-atoms enter into the framework of CN with two different positions: one at the bay carbon site and the other at the corner carbon site (see Fig. S**6**).

Fig. 2 shows the surface morphology and element mapping of $B_{0.1}CN$ and $B_{0.1}CN$/SBA-15, the samples that exhibit the best activity. As expected, $B_{0.1}CN$/SBA-15 shows a 2D hexagonal structure as seen for pristine SBA-15 [36,52], and $B_{0.1}CN$ consists of thin layers

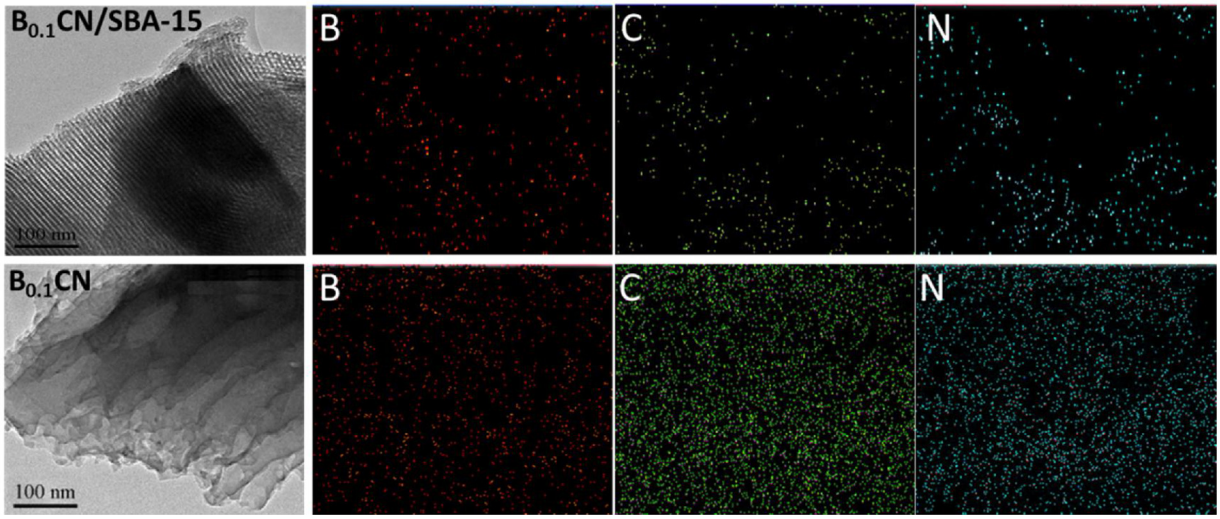


**Fig. 2.** TEM image of $B_{0.1}$CN/SBA-15 (top) and $B_{0.1}$CN (bottom), and the respective element mapping (on the right) of B, C and N atoms obtained from SEM micrographs.

as those of CN [53]. The element mappings from SEM measurements confirm that the B atoms are dispersed in the networks. The images show that the dispersions of B, C and N in $B_{0.1}$CN/SBA-15 (top images) are sparser than those of $B_{0.1}$CN (bottom images), due to the lower overall amount of $B_{0.1}$CN in the supported samples. In some areas, no B, C or N atoms are observed for $B_{0.1}$CN/SBA-15 (e.g., middle of the image), suggesting that the surface of SBA-15 is not fully covered with $B_{0.1}$CN and some places are barren.

### 3.2. Surface basicity and acidity of the materials

$CO_2$- and $NH_3$-TPD measurements were performed in order to evaluate the surface basicity and acidity of the materials, which might later act as adsorption sites for $CO_2$ and SO [33,34]. Fig. 3**A** shows that two apparent $CO_2$ desorption peaks at around 150 and 433 °C appear, indicating the presence of different surface basic sites. The peak area increases significantly from CN to $B_{0.1}$CN, especially for the high temperature peak, this indicates that more surface basic sites are formed after B doping. It is possible that more surface amine groups are generated due to the surface termination caused by $B(OH)_3$ addition, as seen from Fig. S**2** and the XRD patterns. Based on our previous achievements [11], we fitted the $CO_2$-TPD profile into three peaks and assigned them to C—N—C, >NH and —$NH_2$ groups, respectively.

Three separated peaks are observed on the $CO_2$-TPD profile of $B_r$CN/SBA-15, Fig. 3**B**. In terms of CN/SBA-15, the first peak at lower temperatures decreases greatly after the B doping. Possible explanations are: 1) the addition of $B(OH)_3$ neutralizes the surface basicity of SBA-15, which also shows a considerable $CO_2$ desorption peak at 123 °C (Fig. S**7**), and 2) the C—N—C groups are mostly covered by the >NH and —$NH_2$ groups, due to the surface termination. This is supported by the large increase in the area of the second and the third desorption peaks, which are attributed to the >NH and —$NH_2$ groups. It is worth noting that the third peak of both CN/SBA-15 and $B_{0.1}$CN/SBA-15 is large and abnormal, which can perhaps be due to the $CO_2$ physically adsorbed inside the pores (although this cannot be confirmed by the present results). The larger peak area of $B_{0.1}$CN/SBA-15 suggests that it has a larger capacity for $CO_2$ adsorption than CN/SBA-15, thus providing more sites for $CO_2$ activation.

Fig. 3**C** shows the $NH_3$-TPD results used for evaluating the surface acidity. A significant increase in the peak area from CN to $B_{0.1}$CN is observed, indicating that the B doping increases also the surface Lewis acidity of CN. No desorption peak is observed for CN, since it is a base material with abundant basic sites [39]. Two desorption peaks centered at 150 and 335 °C are found for $B_{0.1}$CN, which can be attributed to the $NH_3$ adsorbed on the Lewis acidic B atoms with different chemical statuses.

As expected, a large increase in the $NH_3$ desorption peak is observed from CN/SBA-15 to $B_{0.1}$CN/SBA-15, Fig. 3**D**. Moreover, a small desorption peak is observed for CN/SBA-15, which can be due to the $NH_3$ adsorbed on the pores of SBA-15, since CN does not adsorb $NH_3$ because of its basic properties. It is worth noting that, when comparing $B_{0.1}$CN to $B_{0.1}$CN/SBA-15, a decrease in the desorption temperature is observed. The temperature at 335 °C decreases to 251 °C and that at 150 °C decreases to 105 °C. It is possible that the acidity of $B_{0.1}$CN is partially neutralized by the —OH functionalities of SBA-15, leading to decreased desorption temperature.

To evaluate the overall surface properties of CN and $B_{0.1}$CN, Zeta potential of the materials were performed and the results are presented in Fig. S**8,** which shows that the potential of zero charge ($P_{ZC}$) shifts at lower pH values, and the absolute Zeta potential at each pH value increases after the B doping, indicating that the overall surface acidity and surface stability improves from CN to $B_{0.03}$CN.

**Table 1**
Activities for cycloaddition of $CO_2$ and SO obtained from the varied catalysts.[a]

| Entry | Catalyst | SO conv./% | SC sel./% |
|---|---|---|---|
| 1 | None | 4.5 | 99.0 |
| 2 | SBA-15 | 4.6 | 99.0 |
| 3 | CN | 20.1 | 99.0 |
| 4 | $B_{0.03}$CN | 74.2 | 93.1 |
| 5 | $B_{0.03}$CN[b] | 73.9 | 94.0 |
| 6 | $B_{0.04}$CN | 72.6 | 95.6 |
| 7 | $B_{0.05}$CN | 72.8 | 94.3 |
| 8 | $B_{0.1}$CN | 68.6 | 97.8 |
| 9 | $B_{0.2}$CN | 59.8 | 97.0 |
| 10 | Fe-CN | 66.5 | 94.3 |
| 11 | Zn-CN | 41.1 | 96.0 |
| 12 | CN/SBA-15 | 34.2 | 97.0 |
| 13 | $B_{0.03}$CN/SBA-15 | 87.5 | 97.7 |
| 14 | $B_{0.04}$CN/SBA-15 | 91.0 | 98.0 |
| 15 | $B_{0.05}$CN/SBA-15 | 94.0 | 98.0 |
| 16 | $B_{0.1}$CN/SBA-15 | 97.8 | 96.8 |
| 17 | $B_{0.2}$CN/SBA-15 | 72.3 | 98.5 |

[a] Reaction conditions: 1 mL SO, 130 °C, 3 MPa $CO_2$, 30 mg catalyst, t = 24 h.
[b] Gas atmosphere: 50% $CO_2$/Ar, 3 MPa.

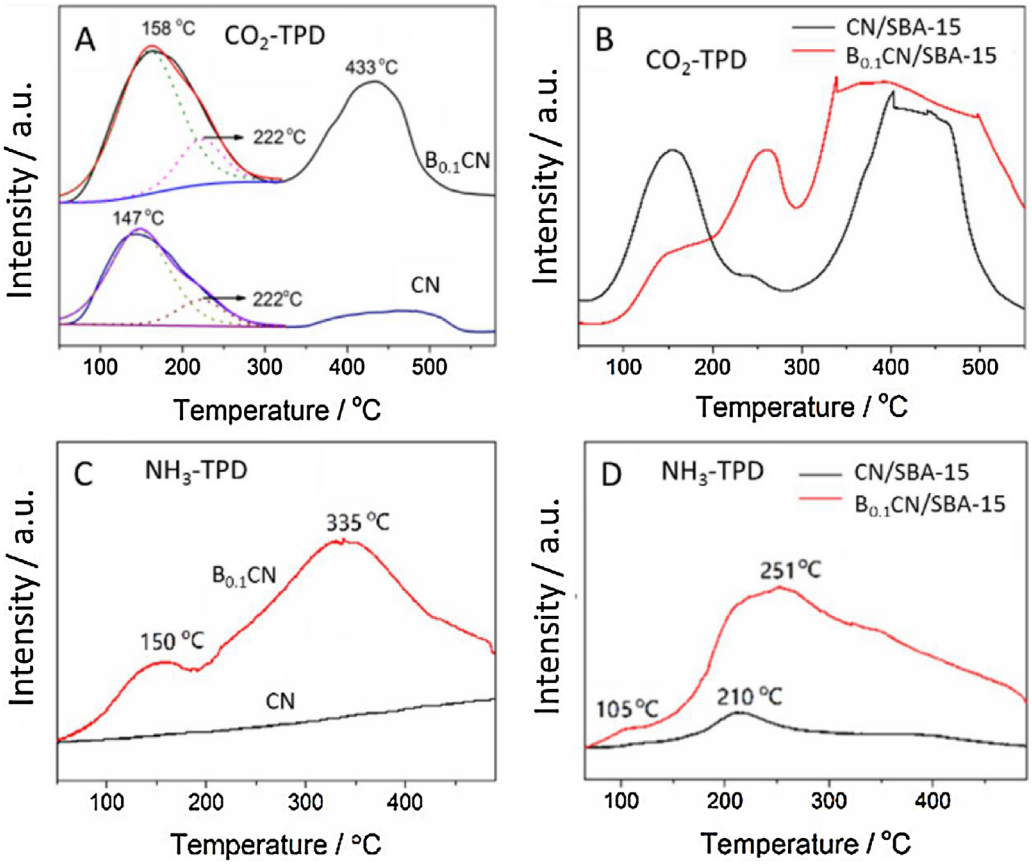


**Fig. 3.** $CO_2$-TPD and $NH_3$-TPD profiles of CN and $B_{0.1}CN$ (A, C), and CN/SBA-15 and $B_{0.1}CN$/SBA-15 (B, D).

### 3.3. Catalytic results

Table 1 lists the SO conversion values found from $CO_2$ and SO cycloaddition reaction over several catalysts. Less than 5% SO conversion is observed after 24 h in the absence of a catalyst. In contrast, 20.1% SO conversion (with a SC selectivity of 99%) is found for CN, which has surface basicity to activate $CO_2$. The SO conversion increases to 34.2% (with a SC selectivity of 97%) when CN/SBA-15 is used, and to 74.2% when a small amount of B atoms are present in the CN, i.e. $B_{0.03}CN$. This shows that both the improvement of surface area and the doping of B atoms (or the presence of acid-base duality) can enhance the activity of CN, and the latter is more pronounced. That is, the co-activation of $CO_2$ and SO is more crucial than solely improve the ability to $CO_2$ activation. As expected, the SO conversion further increases to 87.5% if $B_{0.03}CN$/SBA-15, with high surface area and acid-base duality, is used. SBA-15 alone shows negligible activity to the reaction (see entry 2), thus suggesting that the activity is majorly attributed to the $B_{0.03}CN$ material.

The obtained results show that the best activities are found for $B_{0.03}CN$ and $B_{0.1}CN$/SBA-15, with SO conversions of 74.2% and 97.8%, respectively (SC selectivity above 95% for both cases, see entries 4 and 16). This indicates that the doping of B atoms is essential to the reaction as it can induce the formation of Lewis acid-Lewis base duality, but B doping in excess ($r \geq 0.1$) will degrade the layered structure (see Fig. 1A) and thus hinder the reaction. The different optimal amounts of B doping for $B_{0.03}CN$ and $B_{0.1}CN$/SBA-15 can be attributed to the difference in surface area. For the low-surface-area $B_{0.03}CN$, less $B(OH)_3$ is required for the surface modification to obtain certain amounts of acid-base duality. For the high-surface-area $B_{0.1}CN$/SBA-15, since dicyandiamide is highly dispersed and exposed on SBA-15, more $B(OH)_3$ is required, in order to induce the similar surface density of acid-base duality as that of $B_{0.03}CN$.

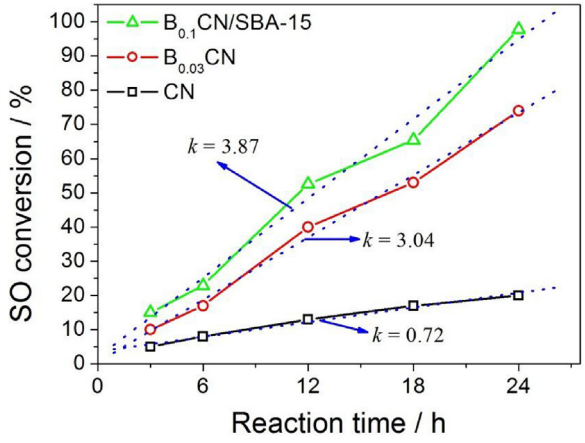


**Fig. 4.** Dependence of SO conversion on the reaction time over the three selected catalysts.

The evolution of the SO conversion with reaction time for the three selected catalysts: CN, $B_{0.03}CN$ and $B_{0.1}CN$/SBA-15, was further carried out to evaluate and compare the reaction rate of SO, and the results are shown in Fig. 4 (Note: the SC selectivity is >90% and not shown here for simplicity; an example is shown in Fig. S**9**). It is interesting to find that the reaction rate of SO increases almost linearly and no plateau appears within the reaction time. This could be to the fact that the reaction is carried out in solvent-free and high pressure (3 MPa) conditions, thus the SO and $CO_2$ can be adsorbed on the active sites and react with each other to yield SC, irrespec-

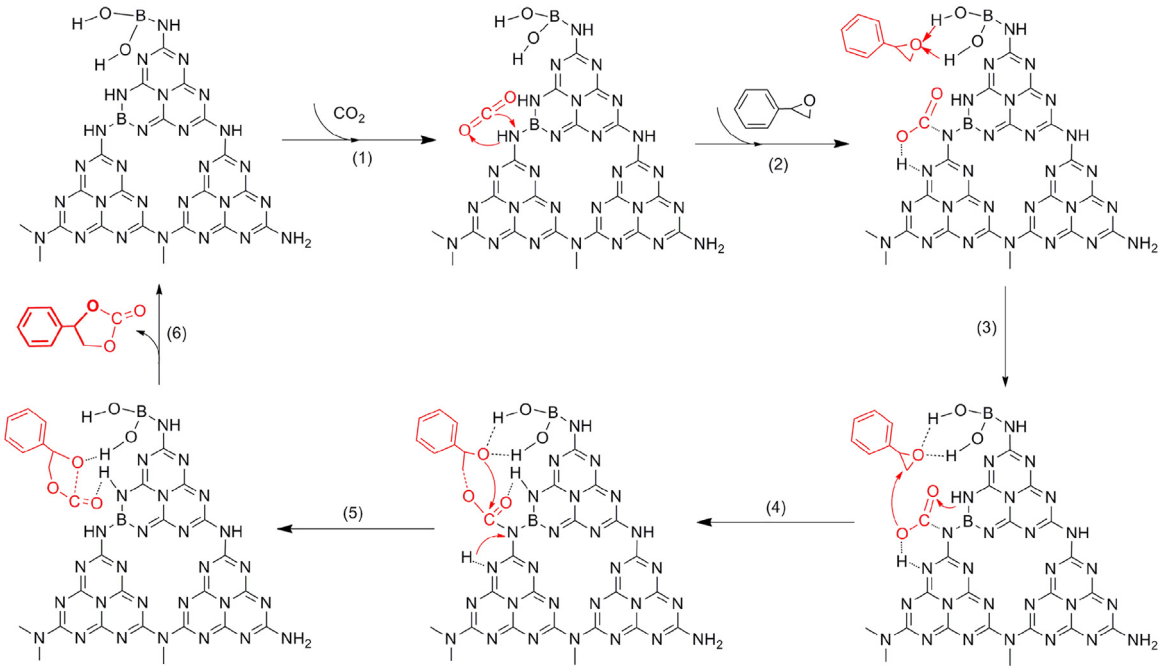


**Scheme 2.** A proposed mechanism for cycloaddition of $CO_2$ and SO on the BCN catalysts.

tive of the decrease in their overall mass with the reaction time. An additional experiment shows that no appreciable change in the activity is observable even at 50% $CO_2$ partial pressure, supporting the above results (see entry 5 of Table 1). The reason can be that the amount of $CO_2$ is in larger excess compared to that of SO, thus the decrease in $CO_2$ mass does not influence much on the reaction. The reaction rate of SO for CN, $B_{0.03}$CN and $B_{0.1}$CN/SBA-15 is 0.72, 3.04 and 3.87 mol $h^{-1}$, respectively. By comparison, it can be seen that the increase of the reaction rate from CN to $B_{0.03}$CN is significantly faster than that from $B_{0.03}$CN to $B_{0.1}$CN/SBA-15, indicating that the presence of an acid-base duality is an intrinsic factor influencing the reaction, and the increase of the surface area improves the reaction by availability of more active sites.

In order to highlight the advantage of $B_{0.1}$CN/SBA-15 for $CO_2$ cycloaddition reactions, we compared its activity with those of several g-$C_3N_4$ based catalysts reported in literature. The results are listed in **Table S1** and show that the present $B_{0.1}$CN/SBA-15 acid-base material is indeed a promising catalyst for $CO_2$ cycloaddition reactions.

Catalytic activity of CN doped with metal ions (i.e., $Fe^{3+}$ and $Zn^{2+}$) was also tested, which shows moderate SO conversion (entries 10 and 11). It is possible that the Fe and Zn atoms do not enter the framework of CN, like B atoms do, and are just coordinated to the N atoms [37], leading to the formation of mainly surface basic sites. On the other hand, when depositing B atoms on the surface of CN or CN/SBA-15 (by impregnation) to yield materials with surface-rich acidic sites, these samples also showed lower activity compared to the B-doped materials, Fig. S**10**, suggesting that surface acidic sites are also not the sole active site of the reaction. Thus, acid-base duality is essential for the reaction.

Further tests show that $B_{0.1}$CN/SBA-15 can be recycled but the activity decreases with the number of cycles performed, Fig. S**11**. This could be partly due to the difficulty of recovering the catalyst, as the products after the reaction are in a gel form, which enwrap the catalyst and penetrate into its pores. Indeed, no destruction of the surface groups of $B_{0.1}$CN is observed even after four cycles of reaction, as verified by the FT-IR spectra, Fig. S**12**. Only a band at 2250 $cm^{-1}$ disappears, possibly is due to the cover of COD. This suggests that the catalyst is stable in the reaction and that the decreased activity observed in the stability tests is attributed to the loss of active sites, physically covered by the reactant or products.

### 3.4. Reaction mechanism

Based on the above discussions and together with the previous achievements on $CO_2$ and epoxides activation over CN and boronic acid [26,31], a reaction mechanism for cycloaddition of $CO_2$ and SO to yield SC over BCN catalysts is proposed, Scheme 2. $CO_2$ is adsorbed on the surface basic >NH sites and activated into carbamate species (step 1), accompanying with the formation of N—C bond and rupture of N—H bond. The ruptured H atoms bonds with an O atom of $CO_2$ and connects to a neighbor N atom by a hydrogen bond (step 2), as proposed by Antonietti et al. [26]. Subsequently, the oxygen of SO adsorbs on the acidic $-B(OH)_2$ sites through a hydrogen bond (step 2), leading to the activation of epoxide, which is then ring-opened by a nucleophilic attack of oxygen anion of the carbamate species (step 3). Meanwhile, a new hydrogen bond between the H atom of >NH in the B—N—C ring and the O atom of $CO_2$ forms in order to weaken the formed O—H bond and facilitate the nucleophilic attack process. The ring-opened oxygen atom of SO will then attack the C atom of $CO_2$ (step 4) to yield the SC (step 5), accompanying the rupture of N—C bond and the return of H atom (to the original N atom). The SC finally desorbs from the surface by breaking the hydrogen bond, regenerating the catalyst (step 6). Because of the presence of base-acid duality (> NH and $-B(OH)_2$), $CO_2$ and SO are co-activated on the BCN surface, promoting the reaction.

In order to support the above conclusions that the doping of B atoms can promote the reaction by co-activation of $CO_2$ and SO, and that the reaction follows a Langmuir-Hinshelwood mechanism, density functional theory (DFT) calculations based on b3lyp/6-31G* algorithm [54] for the reaction were conducted. The optimized models are shown in Fig. 5 and the corresponding data in Table 2 (the optimization process can be found in Fig. S**13**). For $CO_2$, the C=O bond is prolonged after being adsorbed either on CN or BCN, indicating that $CO_2$ can be activated on CN and BCN. The longer bond of C1—O2 (1.216 vs. 1.204) and the lower energy (0.04 vs. 0.60) indicate that the adsorption and activation of $CO_2$ on BCN are

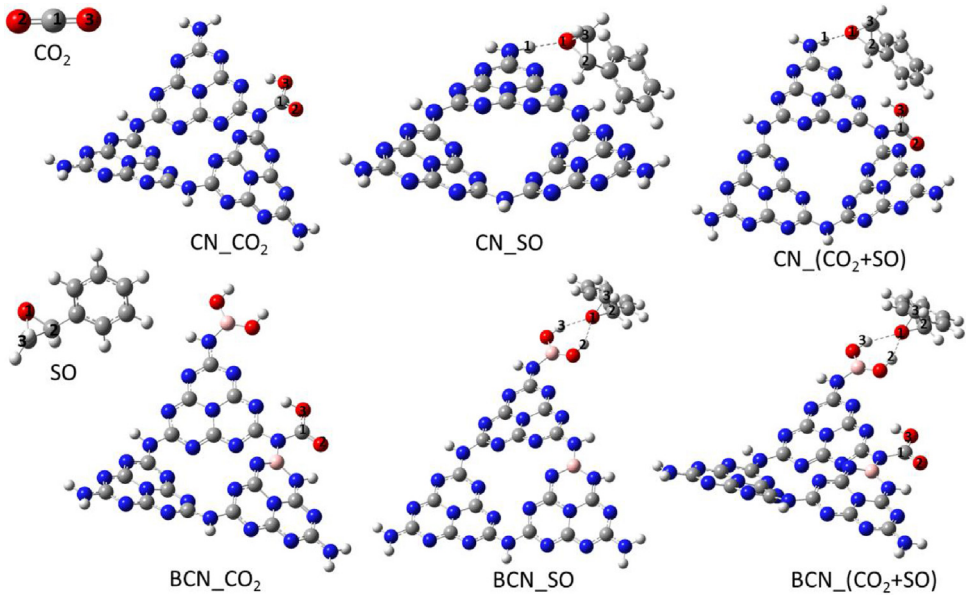


**Fig. 5.** The optimized model for $CO_2$ and SO adsorption/co-adsorption on CN and BCN.

**Table 2**
Changes in the bond length and system energy for $CO_2$ and SO adsorption over CN and BCN. Data obtained from the DFT calculations shown in Fig. 5.

| Model | r (C1-O2) /Å | r (C1-O3) /Å | r (O1-C2) /Å | r (O1-C3) /Å | r (O1-H1/H2) /Å | r (O1-H3) /Å | E /eV |
|---|---|---|---|---|---|---|---|
| $CO_2$ | 1.169 | 1.169 | – | – | – | – | – |
| CN_$CO_2$ | 1.204 | 1.322 | – | – | – | – | 0.60 |
| BCN_$CO_2$ | 1.216 | 1.320 | – | – | – | – | 0.04 |
| SO | – | – | 1.435 | 1.429 | – | – | – |
| CN_SO | – | – | 1.451 | 1.440 | 1.894 | – | −0.42 |
| BCN_SO | – | – | 1.453 | 1.440 | 1.975 | 2.023 | −0.63 |
| CN_($CO_2$ + SO) | 1.204 | 1.325 | 1.454 | 1.439 | 1.899 | – | 0.11 |
| BCN_($CO_2$ + SO) | 1.204 | 1.325 | 1.454 | 1.439 | 1.960 | 2.027 | −0.56 |

more favorable than that on CN. It is worth noting that both energies are above zero, which can be attributed to the energy released from the transfer of hydrogen (the H atom of >NH is transferred to the O3 atom of $CO_2$, accompanying the formation of N—C1 bond, see the models of CN_$CO_2$ and BCN_$CO_2$). That is, the calculated energy contains not only that from the adsorption of $CO_2$, but also that from the transfer of hydrogen. Thus, although $CO_2$ is effectively adsorbed on the catalyst (see the prolonged bond length), the overall energy is above zero.

For SO, only a slight increase in the O—C bond is observed; this is acceptable because it is adsorbed on the catalyst through a weak hydrogen bond, in accordance to what is reported by Wang et al. [31]. Indeed, the calculated bond length of O—H is ranges from 1.894 to 2.023 Å, which is in the range of hydrogen bond values. Although no appreciable change in the O—C bond is observed for SO adsorbed on CN and BCN, a significant difference is found in the O—H hydrogen bond. In the optimized model, only one hydrogen bond forms when SO is adsorbing on CN, while two are formed when SO is adsorbing on BCN, in agreement with the reports of Su et al. [55] and Wang et al. [31]. Because of this difference, SO can be better adsorbed on BCN than that on CN, as verified by the calculated energy (−0.63 vs. −0.42).

From the adsorption energy of $CO_2$ and SO on CN and BCN, we see that the energy change of $CO_2$ is −0.56 eV, and that of SO is −0.21 eV. Taking into account the fast increase of activity from CN to BCN, we infer that $CO_2$ activation would be the rate-determining step of the reaction.

Finally, the overall energy change for the co-adsorption of $CO_2$ and SO on CN and BCN was also calculated and compared (see the last two lines of Table 2). The results show clearly that the BCN is a more favorable catalyst than CN, with an energy change of −0.56 and 0.11, respectively. The above results thus indicate, at least from the energy aspect, that the cycloaddition reaction follows a Langmuir-Hinshelwood mechanism by co-adsorption of $CO_2$ and SO on the catalyst, and the doping of B atoms to CN facilitates the reaction.

## 4. Conclusions

In summary, we report that the doping of B atoms to CN framework significantly increases the surface basicity and surface acidity, which act as active sites of $CO_2$ and SO, respectively. As a result, when $B_r$CN is used for cycloaddition of $CO_2$ and SO, a synergistic effect between the basic and acid sites is induced, leading to enhanced catalytic performances. The activity of $B_r$CN can be further improved if it is supported on high-surface-area SBA-15 (i.e., $B_r$CN/SBA-15), due to the increased contacting area between the catalyst and the reactants, and especially the ability to form more B-containing surface groups. The optimum B contents are 1.09% and 1.61% for $B_r$CN and $B_r$CN/SBA-15, respectively. A mechanism based on acid-base duality acting as active sites of SO and $CO_2$ is proposed, and is supported by the DFT calculations. The excellent activity of $B_r$CN for $CO_2$ cycloaddition reactions opens new vista for the green utilization of $CO_2$.

## Acknowledgments

Financial support from the National Science Foundation of China (21203254), the Natural Science Foundation of Hubei/Liaoning Province of China (2015CFA138/201602681), the Shenyang Normal University Excellent Talent Support Program (51600203), the Shenyang Municipal Science and Technology Planning projects (17-76-1-00), the Portuguese Foundation for Science and Technology (FCT) for Investigador FCT program (IF/01381/2013/CP1160/CT0007), and the Project POCI-01-0145-FEDER-006984–Associate Laboratory LSRE-LCM funded by FEDER through COMPETE2020–POCI–and by FCT, is gratefully acknowledged.

## Appendix A. Supplementary data

Supplementary data associated with this article can be found, in the online version, at http://dx.doi.org/10.1016/j.apcatb.2017.07.041.

## References

[1] M. Yoshida, M. Ihara, Novel methodologies for the synthesis of cyclic carbonates, Chem. Eur. J. 10 (2004) 2886–2893.
[2] J.D. Figueroa, T. Fout, S. Plasynski, H. McIlvried, R.D. Srivastava, Advances in CO2 capture technology—the US department of energy's carbon sequestration program, Int. J. Greenh. Gas Conttrol 2 (2008) 9–20.
[3] A.B. Vidal, L. Feria, J. Evans, Y. Takahashi, P. Liu, K. Nakamura, F. Illas, J.A. Rodriguez, $CO_2$ activation and methanol synthesis on novel Au/TiC and Cu/TiC catalysts, J. Phys. Chem. Lett. 3 (2012) 2275–2280.
[4] M. Tu, R.J. Davis, Cycloaddition of CO2 to epoxides over solid base catalysts, J. Catal. 199 (2001) 85–91.
[5] K.M.K. Yu, I. Curcic, J. Gabriel, H. Morganstewart, S.C. Tsang, Catalytic coupling of CO2 with epoxide over supported and unsupported amines, J. Phys. Chem. A 114 (2010) 3863–3872.
[6] J. Sun, L. Han, W. Cheng, J. Wang, X. Zhang, S. Zhang, Efficient acid–base bifunctional catalysts for the fixation of CO2 with epoxides under metal- and solvent-free conditions, ChemSusChem 4 (2011) 502–507.
[7] T. Sakakura, J.-C. Choi, H. Yasuda, Transformation of carbon dioxide, Chem. Rev. 107 (2007) 2365–2387.
[8] P. Xiao, Y.X. zhao, T. Wang, Y.Y. Zhan, H.H. Wang, J.L. Li, A. Thomas, J.J. Zhu, Polymeric carbon nitride/mesoporous silica composites as catalyst support for Au and Pt nanoparticles, Chem. Eur. J. 20 (2014) 2872–2878.
[9] Q. Yang, W. Wang, Y. Zhao, Y. Zhu, J. Zhu, L. Wang, Metal-free mesoporous carbon nitride catalyze the Friedel-Crafts reaction by activation of benzene, RSC Adv. 5 (2015) 54978–54984.
[10] T. Yuan, H. Gong, K. Kailasam, Y. Zhao, A. Thomas, J. Zhu, Controlling hydrogenation selectivity with Pd catalysts on carbon nitrides functionalized silica, J. Catal. 326 (2015) 38–42.
[11] J.J. Zhu, P. Xiao, H.L. Li, S. Carabineiro, Graphitic carbon nitride: synthesis, properties and applications in catalysis, ACS Appl. Mater. Interfaces 6 (2014) 16449–16465.
[12] J.J. Zhu, Y.C. Wei, W.K. Chen, Z. Zhao, A. Thomas, Graphitic carbon nitride as a metal-free catalyst for NO decomposition, Chem. Commun. 46 (2010) 6965–6967.
[13] X. Wang, S. Blechert, M. Antonietti, Polymeric graphitic carbon nitride for heterogeneous photocatalysis, ACS Catal. 2 (2012) 1596–1606.
[14] Y. Zheng, L. Lin, X. Ye, F. Guo, X. Wang, Helical graphitic carbon nitrides with photocatalytic and optical activities, Angew. Chem. Int. Ed. 53 (2014) 11926–11930.
[15] C. Yang, B. Wang, L. Zhang, L. Yin, X. Wang, Synthesis of layered carbonitrides from biotic molecules for photoredox transformations, Angew. Chem. Int. Ed. 56 (2017) 6627–6631.
[16] G. Zhang, Z.-A. Lan, X. Wang, Conjugated polymers catalysts for photocatalytic hydrogen evolution, Angew. Chem. Int. Ed. 55 (2016) 15712–15727.
[17] D. Zheng, X.-N. Cao, X. Wang, Precise formation of a hollow carbon nitride structure with a janus surface to promote water splitting by photoredox catalysis, Angew. Chem. Int. Ed. 55 (2016) 11512–11516.
[18] H. Ou, L. Lin, Y. Zheng, P. Yang, Y. Fang, X. Wang, Tri-s-triazine-based crystalline carbon nitride nanosheets for an improved hydrogen evolution, Adv. Mater. 29 (2017), http://dx.doi.org/10.1002/adma.201700008 (6 pages).
[19] Y. Cui, G. Zhang, Z. Lin, X. Wang, Condensed and low-defected graphitic carbon nitride with enhanced photocatalytic hydrogen evolution under visible light irradiation, Appl. Catal. B: Environ. 181 (2016) 413–419.
[20] Z.-A. Lan, G. Zhang, X. Wang, A facile synthesis of Br-modified g-$C_3N_4$ semiconductors for photoredox water splitting, Appl. Catal. B: Environ. 192 (2016) 116–125.
[21] J. Qin, S. Wang, H. Ren, Y. Hou, X. Wang, Photocatalytic reduction of $CO_2$ by graphitic carbon nitride polymers derived from urea and barbituric acid, Appl. Catal. B: Environ. 179 (2015) 1–8.
[22] J. Xu, K.-Z. Long, Y. Wang, B. Xue, Y.-X. Li, Fast and facile preparation of metal-doped g-$C_3N_4$ composites for catalytic synthesis of dimethyl carbonate, Appl. Catal. A: Gen. 496 (2015) 1–8.
[23] F. Goettmann, A. Fischer, M. Antonietti, A. Thomas, Metal-free catalysis of sustainable Friedel-Crafts reactions: direct activation of benzene by carbon nitrides to avoid the use of metal chlorides and halogenated compounds, Chem. Commun. 453 (2006) 4530–4532.
[24] F. Goettmann, A. Fischer, M. Antonietti, A. Thomas, Mesoporous graphitic carbon nitride as a versatile, metal-free catalyst for the cyclisation of functional nitriles and alkynes, New J. Chem. 31 (2007) 1455–1460.
[25] P. Zhang, Y. Gong, H. Li, Z. Chen, Y. Wang, Selective oxidation of benzene to phenol by $FeCl_3$/mpg-$C_3N_4$ hybrids, RSC Adv. 3 (2013) 5121–5126.
[26] F. Goettmann, A. Thomas, M. Antonietti, Metal-free activation $CO_2$ by mesoporous graphitic carbon nitride, Angew. Chem. Int. Ed. 46 (2007) 2717–2720.
[27] J. Lin, Z. Pan, X. Wang, Photochemical reduction of $CO_2$ by graphitic carbon nitride polymers, ACS Sustain. Chem. Eng. 2 (2013) 353–358.
[28] Z. Huang, F. Li, B. Chen, T. Lu, Y. Yuan, G. Yuan, Well-dispersed g-$C_3N_4$ nanophases in mesoporous silica channels and their catalytic activity for carbon dioxide activation and conversion, Appl. Catal. B: Environ. 136–137 (2013) 269–277.
[29] J. Xu, J.-K. Shang, Q. Jiang, Y. Wang, Y.-X. Li, Facile alkali-assisted synthesis of g-$C_3N_4$ materials and their high-performance catalytic application in solvent-free cycloaddition of $CO_2$ to epoxides, RSC Adv. 6 (2016) 55382–55392.
[30] J. Xu, F. Wu, Q. Jiang, J.-K. Shang, Y.-X. Li, Metal halides supported on mesoporous carbon nitride as efficient heterogeneous catalysts for the cycloaddition of $CO_2$, J. Mol. Catal. A: Chem. 403 (2015) 77–83.
[31] J. Wang, Y. Zhang, Boronic acids as hydrogen bond donor catalysts for efficient conversion of CO2 into organic carbonate in water, ACS Catal. 6 (2016) 4871–4876.
[32] X.H. Zhang, N. Zhao, W. Wei, Y.H. Sun, Chemical fixation of carbon dioxide to propylene carbonate over amine-functionalized silica catalysts, Catal. Today 115 (2006) 102–106.
[33] K. Yamaguchi, K. Ebitani, T. Yoshida, H. Yoshida, K. Kaneda, Mg-Al mixed oxides as highly active acid-Base catalysts for cycloaddition of carbon dioxide to epoxides, J. Am. Chem. Soc. 121 (1999) 4526–4527.
[34] J. Kim, S.-N. Kim, H.-G. Jang, G. Seo, W.-S. Ahn, CO2 cycloaddition of styrene oxide over MOF catalysts, Appl. Catal. A: Gen. 453 (2013) 175–180.
[35] K. Yamaguchi, K. Ebitani, T. Yoshida, H. Yoshida, K. Kaneda, Mg-Al mixed oxides as highly active acid-base catalysts for cycloaddition of carbon dioxide to epoxides, J. Am. Chem. Soc. 121 (1999) 4526–4527.
[36] D.Y. Zhao, J.L. Feng, Q.S. Huo, N. Melosh, G.H. Fredrickson, B.F. Chmelka, G.D. Stucky, Triblock copolymer syntheses of mesoporous silica with periodic 50–300 angstrom pores, Science 279 (1998) 548–552.
[37] X.C. Wang, X.F. Chen, A. Thomas, X.Z. Fu, M. Antonietti, Metal-containing carbon nitride compounds: a new functional organic-metal hybrid material, Adv. Mater. 21 (2009) 1609–1612.
[38] S.C. Yan, Z.S. Li, Z.G. Zou, Photodegradation of rhodamine B and methyl orange over boron-doped g-C3N4 under visible light irradiation, Langmuir 26 (2010) 3894–3901.
[39] A. Thomas, A. Fischer, F. Goettmann, M. Antonietti, J.-O. Müller, R. Schlögl, J.M. Carlsson, Graphitic carbon nitride materials: variation of structure and morphology and their use as metal-free catalysts, J. Mater. Chem. 18 (2008) 4893–4908.
[40] X. Gouin, P. Grange, L. Bois, P. L'Haridon, Y. Laurent, Characterization of the nitridation process of boric acid, J. Alloys Compd. 224 (1995) 22–28.
[41] X.F. Li, J. Zhang, L.H. Shen, W.W. Lei, D.P. Yang, Q.L. Cui, G.T. Zou, Synthesis and characterization of nanocrystalline hexagonal boron carbo-nitride under high temperature and high pressure, J. Phys.: Condens. Matter. 19 (2007) 425235.
[42] M. Groenewolt, M. Antonietti, Synthesis of g-C3N4 nanoparticles in mesoporous silica host matrices, Adv. Mater. 17 (2005) 1789–1792.
[43] Q. Guo, Y. Xie, X. Wang, S. Zhang, T. Hou, S. Lv, Synthesis of carbon nitride nanotubes with the C3N4 stoichiometry via a benzene-thermal process at low temperatures, Chem. Commun. (2004) 26–27.
[44] V.N. Khabashesku, J.L. Zimmerman, J.L. Margrave, Powder synthesis and characterization of amorphous carbon nitride, Chem. Mater. 12 (2000) 3264–3270.
[45] E.d.S. L. Ansaloni, Boron nitride nanostructured: synthesis, characterization and potential use in cosmetics, Mater. Sci. Appl. 4 (2013) 22–28.
[46] D.L.S.C.M. Su, Coordination of adsorbed boron: a FTIR spectroscopic study, Environ. Sci. Technol. 29 (1995) 302–311.
[47] D. Peak, G.W. Luther III, D.L. Sparks, ATR-FTIR spectroscopic studies of boric acid adsorption on hydrous ferric oxide, Geochim. Cosmochim. Acta 67 (2003) 2551–2560.
[48] Y. Wang, H. Li, J. Yao, X. Wang, M. Antonietti, Synthesis of boron doped polymeric carbon nitride solids and their use as metal-free catalysts for aliphatic C-H bond oxidation, Chem. Sci. 2 (2011) 446–450.
[49] V. Cholet, L. Vandenbulcke, J.P. Rouan, P. Baillif, R. Erre, Characterization of boron nitride films deposited from BCl3-NH3-H2 mixtures in chemical vapour infiltration conditions, J. Mater. Sci. 29 (1994) 1417–1435.

[50] M. Kawaguchi, T. Kawashima, T. Nakajima, Syntheses and structures of new graphite-like materials of composition BCN(H) and $BC_3N(H)$, Chem. Mater. 8 (1996) 1197–1201.
[51] M. Hubáček, T. Sato, T. Ishii, A coexistence of boron nitride and boric oxide, J. Solid State Chem. 109 (1994) 384–390.
[52] J.J. Zhu, K. Kailasam, X. Xie, R. Schomaecker, A. Thomas, High-Surface-Area SBA-15 with enhanced mesopore connectivity by the addition of poly(vinyl alcohol), Chem. Mater. 23 (2011) 2062–2067.
[53] X.C. Wang, K. Maeda, A. Thomas, K. Takanabe, G. Xin, J.M. Carlsson, K. Domen, M. Antonietti, A metal-free polymeric photocatalyst for hydrogen production from water under visible light, Nat. Mater. 8 (2009) 76–80.
[54] M.J. Frisch, G.W. Trucks, H.B. Schlegel, G.E. Scuseria, M.A. Robb, J.R. Cheeseman, et al., Gaussian 09, Revision E. 01, Gaussian Inc., Wallingford CT, 2013.
[55] Q. Su, J. Sun, J. Wang, Z. Yang, W. Cheng, S. Zhang, Urea-derived graphitic carbon nitride as an efficient heterogeneous catalyst for $CO_2$ conversion into cyclic carbonates, Catal. Sci. Technol. 4 (2014) 1556–1562.